Surface & Coatings Technology 402 (2020) 126307

Contents lists available at ScienceDirect

Surface & Coatings Technology

journal homepage: www.elsevier.com/locate/surfcoat

Bioactivation of zirconia surface with laminin protein coating via plasma etching and chemical modification

Lillian V. Tapia-Lopez[a], Hilda E. Esparza-Ponce[a], Antonia Luna-Velasco[a], Perla E. Garcia-Casillas[b], Homero Castro-Carmona[c], Javier S. Castro[b,*]

[a] Centro de Investigación en Materiales Avanzados, Miguel de Cervantes Saavedra 120, Complejo Industrial Chihuahua, 31136, Mexico
[b] Universidad Autónoma de Ciudad Juárez, Av. del Charro 450, Col. Partido Romero, 32310, Mexico
[c] Grupo dental cumbre, Vía Lombardía 5705, Suite 302, Col Saucito, Corporativo Distrito 1, 31110, Mexico

ARTICLE INFO

Keywords:
Surface modification
Protein coating
Bioceramics
Bioactivity
Biofunctionalization

ABSTRACT

Surface modification offers a promising alternative to provide bioactivity to implanted inert biomaterials, improving their integration and performance with living tissues. In this contribution, zirconia has been used as a substrate to investigate the biofunctionalization process, designed to add surface bioactivity to a bioinert biomaterial. We intended to attach laminin-5, known for its ability to bind epithelial cells in soft tissue, to the surface of the extracellular matrix protein. First, the zirconia surface was etched and activated with argon plasma and subsequently it was chemically functionalized with calcium and phosphate ions. Zirconia surface activation was monitored by means of a wettability test, whereas functionalization with calcium and phosphate ions was evaluated by confocal Raman microscopy, Z-potential and X-ray Photoelectron Spectroscopy (XPS). The binding of laminin-5 protein to the zirconia surface was carried out by means of adsorption and confirmed by XPS. Then, we used SEM and AFM to observe a homogeneous covering of globular protein over the zirconia surface. Furthermore, epithelial cell response over zirconia surfaces was assayed to show that biofunctionalized surfaces enhance cell adhesion to a greater extent than substrates without protein coating. Our results indicate how the zirconia surface can be modified using argon plasma, in order to enable its bioactivation with the laminin-5 protein.

1. Introduction

Bioceramics are materials used mostly for medical applications such as implantable devices and body part replacements, due to their biocompatibility and mechanical properties [1].

However most ceramics are bioinert, meaning that they do not interact with surrounding soft or hard tissues [2–4]. This lack of bioactive interaction at the site of implantation can produce fibrous encapsulation of the foreign body [5,6], chronic pain or discomfort, loss of functionality, acute or chronic inflammation, tissue damage [6,7], shifting of the implant [8] and aseptic loosening [9]. Modern biomedicine requires improved biomaterials, capable of interacting positively with their biological environment in different ways [10], for instance by forming strong bonds with tissues, adapting to physical or physiological changes, [10,11], reacting to changes in pH or temperature [12] etc. A biomaterial that manifests any of these characteristics can be considered as bioactive [10]. Hence, biomaterial researchers have two options, to fabricate novel bioactive materials [13] or to modify the surface of existing ones, as most implant tissue interactions take place at the surface. There has therefore been a tendency to modify the surface of inert biomaterials, with the intention of adding bioactivity [3,9,14,15]. The most common and successful has been bioactivation to promote the bond with hard tissue (bone), for instance titanium hip implants fixed with cement have been substituted with bioactive implants made of titanium, functionalized with hydroxyapatite, in order to promote osteo-integration with bone, thus avoiding a common failure known as aseptic loosening [16]; likewise titanium dental implants have been functionalized in the same way, resulting in improved fixation (Nobel Biocare, Zurich, Switzerland). However, the bonding implant-soft tissue has barely been studied. In this contribution, we are proposing a biofunctionalization method for zirconia that in the future will facilitate the implant-soft tissue bond in hard materials used as bone substitutes. Zirconia (3Y-TZP) was chosen as a model material because it is one of the most used bioceramics in areas such as orthopedics and dentistry [3,17], due to its biocompatibility, mechanical strength, aesthetic appearance [17,18], low bacterial affinity [3] and

* Corresponding author.
E-mail address: jcastro@uacj.mx (J.S. Castro).

https://doi.org/10.1016/j.surfcoat.2020.126307
Received 13 May 2020; Received in revised form 13 August 2020; Accepted 15 August 2020
Available online 18 August 2020
0257-8972/

wear resistance [4]. However there are scarce reports about zirconia biofunctionalization [19,20] and to our knowledge, neither is there any bioactive zirconia in the biomedical market. Biofunctionalized zirconia could be used in several biomedical applications, where a bioactive bond with soft tissue is important, for instance in dentistry it may improve the effectiveness of current abutments, promoting a biological bond with the gingival epithelium, sealing the interfase abutment-epithelium; consequently helping avoid infection caused by bacteria infiltration known as peri-implantitis; a common problem in dental implants [21,22]. Moreover bioactive zirconia may improve traditional orthopedic uses or even offer new applications in related facial surgery for example aesthetic, maxillofacial or cranial surgery.

Bioactivity can be implemented by functionalization with bioactive materials i.e. based on calcium phosphates [3,14] or biofunctionalization with biomolecules like polypeptides and proteins [19,20]. The bioactive layer which is designed to be deposited over the surface of a previously fabricated biomaterial is usually very different in composition and affinity; however several processing techniques can be applied to remedy this problem. Sandblasting, polishing, UV, laser, plasma, alkaline and acid treatments [17,19] are some of the most commonly used. These modify surfaces by cleaning, etching, oxidizing or providing polar reactive groups (e.g. OH^-) [17,19,23].

Among these techniques, plasma treatment is gaining attention because it is a solvent-free technique, which is capable of modifying surface properties without affecting the bulk characteristics of the material, as occurs when surface activation is induced by the introduction or substitution of functional groups [24–26]. Subsequently functionalization with bioactive molecules, sterilization [24] and change in surface texturing [26,27].

Specifically, activation of zirconia surfaces with plasma has been reported by Fernandez et al. who used air plasma to facilitate a silanization reaction that enabled the binding of a peptide to improve osteoblast cell adhesion to zirconia surfaces [19]. Similarly, Caravaca et al. used oxygen plasma to cause direct silanization of the zirconia surface, in order to improve the adhesion response of osteoblast-like cells [23].

With regard to surface biofunctionalization, biomolecules are chosen, depending on the application required and the methods of adhesion to the surface are usually chemically or physically immobilized [19,20,28]. To mention some examples, collagen has been used to enhance the spreading, viability and attachment of endothelial cells for vascular graft applications [29]. Fibronectin coating has been used to attach and proliferate arterial endothelial cells [30].

In this work, our aim is to attach epithelial cells to the zirconia surface, aspiring to improve implant tissue interactions in the case of the zirconia-epithelium interface. For this, laminin-5 (Ln-5) was chosen because it is a well-known epithelial cell-adhesive protein that includes a domain which binds to the extracellular matrix via integrins [31,32], meaning that Ln-5 may improve cell adhesion to the bioceramic surface. As reference, a previous study of the interactions of Ln-5 over alumina-zirconia has demonstrated better epithelial cell activation on the surface functionalized with the protein, than on those that remained unfunctionalized [20].

Considering the latter outcomes, we believe zirconia biofunctionalization with Ln-5 protein, by means of argon plasma activation and chemical processing with calcium and phosphate ions in order to improve surface bioactivity is feasible and necessary to improve interaction with biological systems. Therefore, the aim of this study is to provide a suitable process for the biofunctionalization of inert bioceramics such as zirconia, with promising implant applications.

2. Materials and methods

2.1. Zirconia sample preparation

A dental pre-sintered zirconia Natura Zir® 3Y-TZP, acquired from Ideas Dentales (Mexico City, Mexico), was used to produce discs of 16 mm for contact angle measurements, 6 mm for the viability assay and 8 mm for all other assessments. All discs were 3 mm in thickness. The discs where designed in SolidWorks© software and milled in a dental milling machine, Roland DWX-51D (Hamamatsu, Japan). Then, the discs were completely sintered at 1500 °C in a furnace, Duotron Pro (Gyeonggi, Korea), according to supplier specifications (untreated sample). Once sintered, disc surfaces were ground with a 9 μm diamond paper for 5 min and polished for 5 min, using a diamond suspension (1 μm particle size) on nylon pads in a rotator GPX 200 Leco polisher at 250 rpm (Maharashtra, India). This process was undertaken to smooth the ceramic surface in order to favor protein and cell adhesion [33]. Finally, the polished samples were sonicated in pure water, acetone and ethanol for 10 min each, in order to remove any residues from the grinding and polishing.

2.2. Plasma surface treatment

Argon plasma treatment of polished samples was used to activate their surfaces increasing surface energy and reactivity [34,35] for a successful chemical functionalization. This happens because plasma is able to create reactive sites by breaking atomic bonds [27] and incorporating oxygen containing functional groups [25], possibly reducing some contaminants [35,36]. In addition, plasma produces a mild etching effect on the surface that it may help to smooth the surface. The process was carried out in a low pressure plasma system from Diener Plasma Technology model Femto Standard Version (Ebhausen, Germany).

Sample surfaces were treated with argon plasma for 20 min, at 0.4 mbar pressure, voltage supply 220 V, power 70 W (0–100 W), vacuum pump speed 1.5 m^3/h, gas flow 10 sccm and generator frequency 40 kHz. The pressure and power parameters were adjusted according to the manufacturer specifications for the activation of ceramics. These samples were denominated plasma-treated, a treatment which was implemented to assist functionalization. Argon was chosen because it does not react with the surface.

2.3. Surface functionalization

Functionalization with calcium and phosphate ions was undertaken in a two-step process as reported by Sunarso et al. [14]. Following a 20 min time period post plasma treatment, plasma-treated samples were immersed in 0.1 M $NaH_2PO_4{\cdot}H_{2O}$ aqueous solution (pH 5) at 80 °C, for 24 h. Then, samples were rinsed in an ultrasonic bath with ultrapure water, ethanol and acetone, for 4 min each. Subsequently, samples were immersed in a second solution of 0.01 M $CaCl_2$ (pH 6.8) at 80 °C for 1 h. Next, samples were thoroughly rinsed; first with ultra-pure water and then with acetone. Finally, they were dried at 100 °C for 15 min and stored in a dry environment for subsequent characterization. These samples were identified as plasma-CaPhos. Polished samples without plasma treatment were also functionalized as reference controls, denominated CaPhos. In this section the experiments were conducted in duplicate. Functionalization steps can be chemically explained as follows: 1) The dissociation of monosodium phosphate ($NaH_2PO_4{\cdot}H_2O$) (Eq. (1)) at pH 5 enables the chemical bonding of phosphate ion to the activated Zr on the surface of ceramic substrate by electrostatic interactions (Eq. (2)).

$$NaH_2PO_4.\ H_2O + H_2O \rightarrow HPO_4^{2-} + Na^+ + 2H_3O^+ \quad (1)$$

$$HPO_4^{2-} + Zr_{surface} \xrightarrow[80°C,24\ h]{} Zr_{suface}HPO_4^{2-} \quad (2)$$

2) The Ca^{2+} ions provided by $CaCl_2$ solution (Eq. (3)) are able to electrostatically interact with phosphates deposited on the ceramic surface or with surface activated O^- atoms in the substrate, forming calcium-phosphate-zirconium and Ca-oxygen bonds (Eq. (4)).

$$CaCl_2 \rightarrow Ca^{2+} + 2Cl^- \quad (3)$$

$$Zr_{surface}HPO_4^{2-} + Ca^{2+} + O^-_{surface} \xrightarrow[80°C,1\ h]{} Ca(HPO_4)Zr_{surface} + CaO_{surface} \quad (4)$$

2.4. Biofunctionalization with Ln-5

Ln-5 protein was acquired from BioLamina (Matawan, NJ, USA), at a concentration of 0.16 μM in a PBS solution containing 10% glycerol and 0.02% NaN_3, pH 7.2. The protein solution was aliquoted as received and stored at −20 °C. Within 24 h following functionalization with calcium and phosphate ions, the plasma-CaPhos samples were treated with argon plasma at 0.4 mbar pressure for 2 min. This process does not affect functionalization substantially, instead plasma increases reactivity breaking atomic bonds and introducing oxygen incorporating functional groups (see XPS results in Table I supplementary). Then, the samples were covered with 10 μL of 0.08 μM or 0.016 μM protein solution, and kept for 2 h at 37 °C, under aseptic conditions. These protein solutions were made by diluting the acquired solution in PBS pH 7.4. The samples were denominated Plasma-CaPhos-Ln. Polished and plasma-treated samples (20 min after plasma treatment), were also covered with protein. The experiments were conducted in triplicate to strength reliability.

Additionally, to ensure the stability and attachment of the laminin coating, all protein-covered samples were thoroughly rinsed five times with PBS solution; air dried at 25 °C in a laminar flow chamber and kept under aseptic conditions at 4 °C, until characterization.

2.5. In vitro cellular assays

2.5.1. Cell culture

Epithelial cells (CaCo2; ATCC HTB-37) were cultured in Dulbecco's modified essential medium (DMEM) (ATCC), supplemented with 10% Fetal Bovine Serum FBS (ATCC). Cells were stored at 37 °C at 5% CO2 in an incubator, maintaining a minimum of 80% humidification. Passes were made every 2–3 days, depending on cellular confluence. Confluent cells were detached using 0.05% Trypsin-EDTA solution (Sigma Aldrich).

2.5.2. Cell viability (MTT)

We determined the viability of cells deposited on ceramic samples with an MTT assay. MTT is an indicative test for measuring cell metabolic activity. Reduced to a purple formazan salt, this provides a quantifiable marker for living cells [37]. The assay was performed on fully treated ceramic samples where protein was deposited (plasma-CaPhos-Ln 0.08 μM), as well as on samples partially treated without protein as reference (polished, plasma-treated, plasma-CaPhos). A positive control, consisting of 1.5×10^4 cells/well-seeded in a treated plate was taken as reference for cell viability. Disc samples were placed in a 96-well plate and the cells were seeded at a density of 1.5×10^4 cells/well and then, DMEM supplemented with 10% FBS were added, reaching a final volume of 200 μL. The 96-well plate was incubated for 20 h at 37 °C and 5% CO_2 atmosphere. Subsequently, culture medium was withdrawn from the wells and gently washed once with PBS. Next, 200 μL of DMEM and MTT (0.5 mg/mL in PBS) were added to each well. The microplates were protected from light and incubated at 37 °C for 4 h at 5% CO_2. The medium was withdrawn from the wells and the resulting formazan crystals were solubilized in 200 μL of acidified isopropanol per well. Posteriorly, 100 μL from each well were transferred to a new 96-well plate and the absorbance was read at 570 nm in a microplate reader Varioskan Lux VLBLATD2, Thermo Fisher Scientific (Massachusetts, USA). All treatments were analyzed in triplicate. Cell viability of a sample was reported as a percentage of optical density, considering the optical density of the positive control to represent 100% viability.

$$\%\text{Viability} = \frac{\text{Optical Density of Sample}}{\text{Optical Density of Positive Control}} \times 100$$

2.5.3. Cell adhesion

Cell adhesion was evaluated for polished, plasma-treated, plasma-CaPhos and plasma-CaPhos-Ln (0.08 μM) samples. For this, samples were placed in a 24-well culture dishes and CaCo2 cells (1.5×10^4 cells/well) were seeded on the surface of each sample. Then DEMEM, supplemented with 10% of FBS were added to each well, reaching a final volume of 2 mL. The samples were incubated for 24 h at 37 °C and 5% CO_2 atmosphere. This step allows the cells to adhere, grow and proliferate at the surface of the samples. Following incubation, the cells were washed with PBS and then fixed with paraformaldehyde solution (3.75%; 20 min) at 4 °C, permeabilized with triton X-100 (0.5%; 10 min) and blocked with lacteous protein (10%; 1 h), at room temperature. For F-actin staining, phalloidin (acquired from Biotium CF®488A, Fremont, CA, USA) was used to cover the sample surface for 20 min at room temperature. Then, samples were gently washed with PBS and each surface was covered with Hoechst (for nucleus staining) for 30 min at 37 °C. Lastly, surface samples were gently washed twice with PBS and analyzed using a confocal fluorescence microscope (Zeiss LSM-700, Jena, Germany). We counted the number of adhered cells visible in confocal images, analyzing four images per sample and three different samples per group (field area of 0.4098 mm^2), using the Image J software (NIH, USA). The amplification was 20×.

2.6. Characterization of zirconia surfaces

Static water contact angles were measured at room temperature on plasma-treated plasma-CaPhos, polished and untreated (unpolished) samples, using FTA200 wettability equipment (Virginia, USA). Measurements were taken after 20 min in the case of each treatment and likewise, the plasma-treated sample was measured after 48 h, for comparison. A distilled water drop of 2 μL was automatically deposited on the sample surfaces using a surgical syringe with a precision flow control valve. Measurements of the static contact angle were automatic, using FTA image analysis software. For each sample, 3 contact angles were measured and an average value was calculated. Standard deviations varied from 3° to 5°.

The x-y-z-topography of the samples surfaces was extracted and the root mean square (RMS) roughness was calculated, using an atomic force microscope (AFM) MPF-3D Infinity Asylum Research (Oxford, England) in tapping mode, with PPP-EFM nanosensors 2.5 Nw/M tips. Scanning area of $500 \times 500\ nm^2$, at a rate of 0.76 Hz and pixel size of 19.6 nm. For imaging mode, a setpoint of 646.75 mV, drive amplitude of 39.52 mV and drive frequency of 76.554 kHz were implemented.

A confocal Raman alpha 300R microscope Witec (Ulm, Germany) was used for analyzing plasma-CaPhos to detect calcium-phosphate. CaPhos and polished samples were also analyzed as reference controls. This was equipped with a frequency doubled NdYAG laser of 532 nm, a high throughput UHTS spectrometer and a CCD camera, optimized for the excitation laser. The Raman spectral measurements were carried out using f/4300 mm focal length imaging spectrometer with a 20× objective lens. All Raman spectra were recorded in the regions of 2000–0 cm^{-1}. Also, Atomic Force microscope alpha 300 A from the same manufacturer was used to map small surface areas (10 × 10 microns) of the plasma-CaPhos sample, with lateral and depth resolutions < 1 nm and < 0.3 nm, respectively.

X-ray Photoelectron Spectroscopy (XPS) was used to determine the elements present on all sample surfaces, employing a Thermo Scientific Escalab 250xi instrument (Massachusetts, USA), equipped with a monochromatic Al Kα X-ray source ($h\nu$ = 1486.86 eV) and 0.4–0.6 eV resolution. An electron flood gun was set at 10 eV, spot size 650 μm, energy step size 1.00 eV, lens mode standard, analyzer mode: pass energy 200 eV. All samples from the various surface treatments were

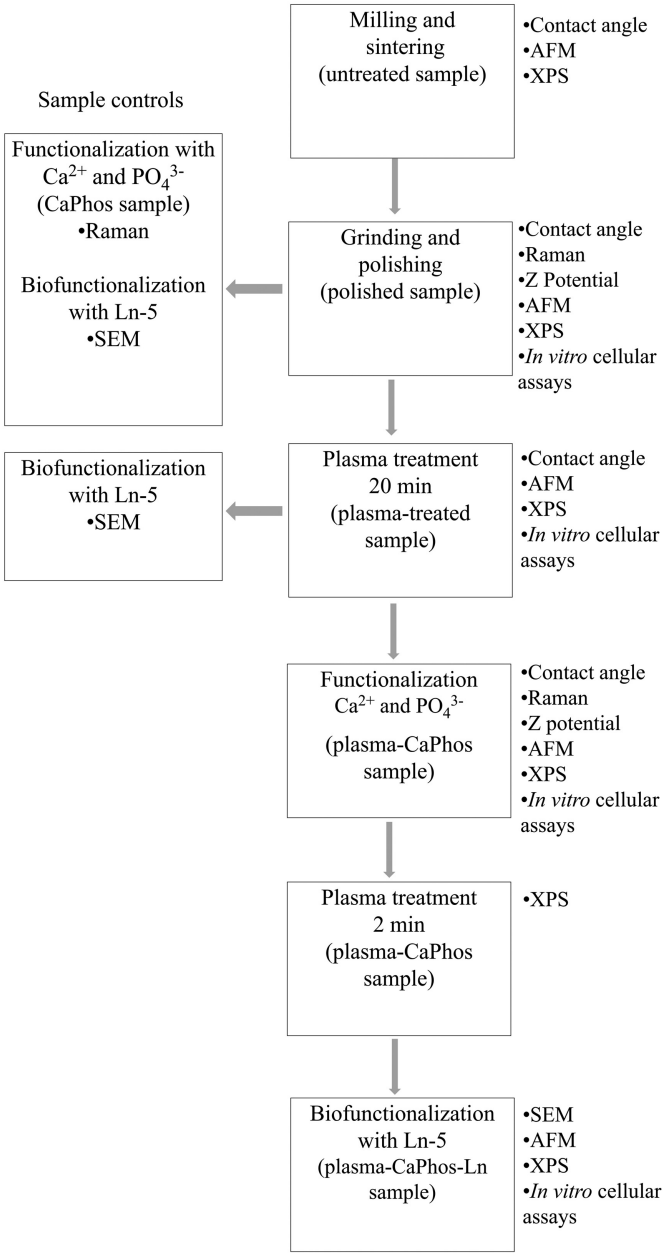

Fig. 1. Schematic process flow with characterization techniques.

measured after 48 h.

The zeta potential of untreated and plasma-CaPhos samples was measured by means of Zetasizer Nano Zs (Malvern, UK), equipped with a gap cell with palladium electrodes, light source He-Ne laser 633 nm and DPSS 10 mW, Power 100VA, temperature 25 °C, 0.001 M KCl electrolyte solution pH 7.2. A total of 30 measurements were taken of each sample surface.

Surface morphology of samples was analyzed by scanning electron microscopy (SEM), using a JEOL 7401 JSM microscope (Tokyo, Japan). Magnification: 10, 20 and 30 kX, accelerating voltage 3 kV, probe current 9 to 10 μA, field emission electron gun (Tungsten tip emitter), ultra-high vacuum.

Finally, XPS analysis was also performed in biofunctionalized samples under a depth profile ion energy, 2000 eV/current, Mid/Raster size of 2 mm and 17 erosion of 4 s each (0.3 nm/s).

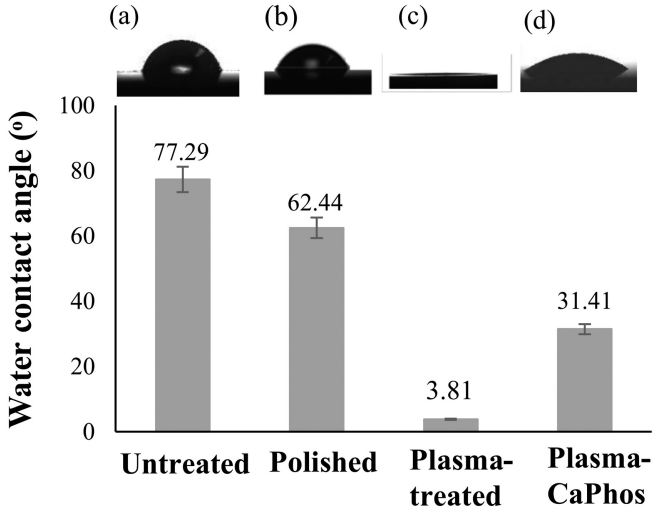

Fig. 2. Water contact angle measurements for surface samples, (a) Untreated, (b) Polished, (c) Plasma-treated and (d) Plasma-CaPhos. Mean values are the average of triplicate values and bars represent standard deviation. The lower the water contact angle, the higher the surface wettability.

2.7. Process flow for zirconia biofunctionalization (Fig. 1)

3. Results and discussion

3.1. Plasma surface treatment

3.1.1. Wettability of sample surfaces

The effect of plasma treatment over the zirconia surface (plasma-treated sample) was analyzed by contact angle technique. The wettability of untreated (unpolished) and polished samples was also measured for comparative purposes. Averaged contact angle measurements (Fig. 2) revealed much higher values for untreated and polished samples, 77.29° (± 5.34°) and 62.44° (± 2.51°) respectively, than for plasma-treated samples 3.81° (± 0.17°). This means that, untreated samples are not wettable at all, as the cohesive forces between water molecules still exceed the adhesive forces between the water drop and the surfaces; as indicated by the form of the water drop on these surfaces (Fig. 2a and b). However, on the plasma-treated samples (Fig. 2c) the water drop spreads, indicating that the surface acquires a higher surface free energy, resulting in a much lower contact angle and thus greater wettability. Zirconia has a surface, for which the basic (negative) and acid (positive) sites are contiguous, presenting, in overall, a very slightly negative charge [38]. When argon plasma is applied, it leaves a highly temporal reactive sites, where O atoms are incorporated [25,27], leading to a higher polar [34,35] and more hydrophilic surface [27]. Plasma also reduced adsorbed hydrocarbon content by breaking C—H and C—C bonds [35,36].

In addition, contact angle measurements made on plasma-treated sample after 48 h showed an increase in the contact angle from 3.81° (± 0.17°) to 48.04° (± 7.2°). This indicates that plasma imposed hydrophilicity is time related and only lasts for limited periods.

3.2. Surface functionalization

3.2.1. Calcium and phosphate

Confocal Raman measurements were carried out on functionalized plasma-treated samples (plasma-CaPhos). Functionalized non plasma-treatment samples (CaPhos) and polished samples (non-functionalized) were also analyzed as reference controls. The Raman spectra of the three samples are shown in Fig. 3a. The polished and CaPhos samples

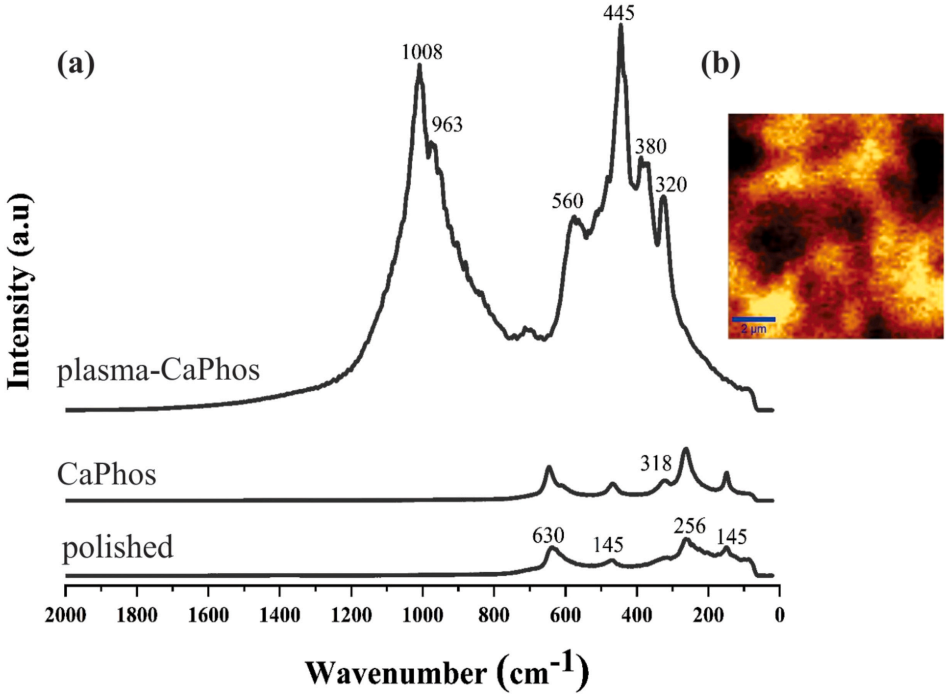

Fig. 3. (a) Raman spectra for functionalized samples with calcium and phosphate. (b) Distribution map of the signal O—P—O at a surface area (10 × 10 μm^2) of the Plasma-CaPhos sample, obtained by Raman mapping. Brighter areas signify greater concentration of the chemical species. Bar length equals 2 µm.

only presented the bands characteristic of tetragonal zirconia 3Y-TZP, around 630, 465, 318, 256 and 145 cm^{-1} [39]. Thus, we can conclude that firstly, the lack of argon plasma treatment on the zirconia surface prohibits their functionalization with calcium and phosphate. On the other hand, this treatment assists functionalization because it increases the polarity of the surface by breaking bonds and incorporating O atoms through polar functional groups which results in greater surface energy and reactivity.

Secondly, the Plasma-CaPhos sample shows a spectrum with two predominant bands, at 1008 $cm^{-1,}$ and 445 cm^{-1} and other smaller bands at 963, 563, 380 and 320 cm^{-1}. The following phosphate vibrational modes have been reported in the literature for calcium phosphate compounds. The asymmetric stretching mode P—O *v3* is found at 1008 cm^{-1} [40,41]. The symmetric bending modes O—P—O *v2* are found at 445 cm^{-1} [41,42] The symmetric stretching modes P—O *v1* are found at 963 cm^{-1} [40,43], whereas, the O—P—O *v4* asymmetric bending modes are found at 563 cm^{-1} [40,41]. The band at 380 cm^{-1} has been reported as a characteristic peak for the dicalcium phosphate dihydrate compound [43] and the 320 cm^{-1} band is characteristic of tetragonal zirconia [39]. Thus, the Raman spectra endorsed the presence of Ca and P elements on the surface of the Plasma-CaPhos sample.

To corroborate the presence of functionalized species at the surface of the plasma-CaPhos sample, three different surface areas of 10 × 10 μm^2 were mapped at the wave number of one of the prominent bands of 445 cm^{-1}, characteristic of a phosphate bending vibration O—P—O. Fig. 3b presents a distribution map of the bending Raman vibration O-P-O, confirming that phosphate is distributed over almost all surfaces at greater and lesser amounts, corresponding to bright and dark areas, respectively. The undetectable signal in the darker areas is probably due to a thinner layer of that species. Mapping was also performed at the less prominent Raman band of 380 cm^{-1} for a dicalcium species, but very low signal strength was detected.

3.2.2. Chemical composition of functionalized zirconia

XPS elemental quantification of untreated, polished, plasma-treated and plasma-CaPhos samples is presented in Table I. The characteristic elements of zirconia (Zr, O and Y) were detected in all samples. In plasma-treated samples, the oxygen content increased due to the effect of plasma over the surface [25,27,35]. The additional elements, Ca2p and P2p, were detected in the plasma-CaPhos sample. C1s is also detected in all samples and the untreated one is the most obviously contaminated, which may come from the sinterization process [38] or from the environment [20]. Similarly, the plasma-treated sample showed the least amount because plasma breaks C—C bonds, resulting in a cleaner surface [34–36].

In order to obtain further insight concerning the chemical bonds present on the zirconia surfaces, the binding energies at Zr3d and O1s on polished, plasma-treated and plasma-CaPhos samples and for Ca2p and P2p on plasma-CaPhos sample were analyzed, Fig. 4. The Zr3d peaks, for all samples, were divided into two doublets of the Zr3d5/2 and Zr3d3/2 peaks located around 182.2 and 184.6, respectively, related to Zr—O bonds. In polished and plasma-CaPhos samples the peaks maintain intensity ratios of 3:2 [35]. In plasma-treated sample an additional peak at higher binding energy (186.8 eV) is detected, related also to Zr—O (Zr3d3/2). The O1s spectra of the polished sample were divided into two peaks at Zr—O peak (530 eV) and OH peak (532.1 eV). For the plasma-treated sample, the O1s peaks were divided into three peaks, a small peak which corresponds to Zr—O (529.6 eV), a peak denoted as OH (532 eV) [35] and the C—O/OH peak (533.3 eV) [23,35]. In this sample, the introduction of O was supported mainly through the OH functional group. Apparently, the Zr—O peak manifests reduced intensity.

For the plasma-CaPhos sample, analyzed by NIST X-ray Photoelectron Spectroscopy Database, the peaks for O1s are shown at 529.9 eV, 531.4 eV and 533.2 eV, corresponding to the bonds for Zr—O, Ca—O/P—O—Ca, and a hydrated surface layer, respectively. In this sample, new binding energies are apparent. The binding energies, characteristic of Ca2p are made evident by the four peaks at 345.9 eV, 346.8 eV, 347.2 eV and 350.9 eV. All peaks are related to Ca- O bonds and the (347.2 eV) peak is also related to the Ca—O—P bond. Likewise, two peaks with the characteristic binding energies for P2p are shown at the P—O—Ca peak (133.8 eV) and P—O—Zr peak (134.3 eV).

Based on these results, the modification of zirconia surface by argon plasma indicates a decrease in C and an increase in O by the incorporation of the OH [35] and C—O functional groups [25,27,35]. This can be attributed to the plasma effect, which may breaks atomic bonds on the surface, creating reactive sites leading to the creation of the latter oxygen functional groups. The increase in these polar components

Table I
Atomic percentage of elements detected by XPS on zirconia surfaces.

Sample	Atomic %					
	Ca2p	P2p	Zr3d	O1s	Y3d	C1s
Untreated	–	–	16.0 ± 6.9	40.4 ± 1.8	2.2 ± 1.3	41.3 ± 6.4
Polished	–	–	15.8 ± 0.3	53.97 ± 0.04	1.3 ± 0.09	28.8 ± 0.03
Plasma-treated	–	–	11.9 ± 4.8	73.11 ± 3.1	2.04 ± 0.4	12.9 ± 2.1
Plasma-CaPhos	10.3 ± 0.8	1.8 ± 0.5	16.1 ± 1.3	52.3 ± 2.5	1.1 ± 0.1	18.1 ± 0.7

on the zirconia surface enhances surface energy and reactivity that enables functionalization with Ca and Phosphate ions.

Functionalization was demonstrated by the detection of Ca and P over the plasma-CaPhos sample and also by the identification of Ca−O−P, P−O−Zr and Ca−O bonds.

A schematic illustration of the suggested bonds present at the zirconia surface after the functionalization process is presented in Fig. 5. The binding of calcium and phosphorous to the surface may be partially ionic and electrostatic. A similar interaction was reported by Sunarso et al. [14], but with titanium disc as substrate.

The modification of surface chemistry generally involves changes in surface properties such as charge and wettability. The surface charge known as surface zeta potential and wettability were measured on plasma-CaPhos and polished samples (non-functionalized). The overall surface zeta potential (at pH 7.2) for plasma-CaPhos samples was −19.5 mV, whereas a much lower value was obtained for non-functionalized samples (−0.13 mV). The increased negative surface charge indicates functionalization with calcium-phosphate. This is consistent with Raman results, where peaks for calcium-phosphate compounds were only detected on the plasma-CaPhos sample and XPS confirmed the binding energies of this chemical association.

3.2.3. Wettability of functionalized samples

To determine the wettability of the functionalized samples (plasma-CaPhos), the water contact angle was measured after 30 min of the functionalization process. Surface wettability is important as it relates to the adhesion capacity of the surface, which is essential for biofunctionalization. The water contact angle determined on plasma-CaPhos samples was 31.41° (± 3.03°), representing a wettable surface, made evident by the flat shape of the drop (Fig. 2d). Thus, the adhesion capacity of plasma-CaPhos zirconia surface is adequate for biofunctionalization with Ln-5.

3.2.4. Zirconia surfaces

Before protein biofunctionalization, it is very important to know how the surface topography is, and how it could interact positively or

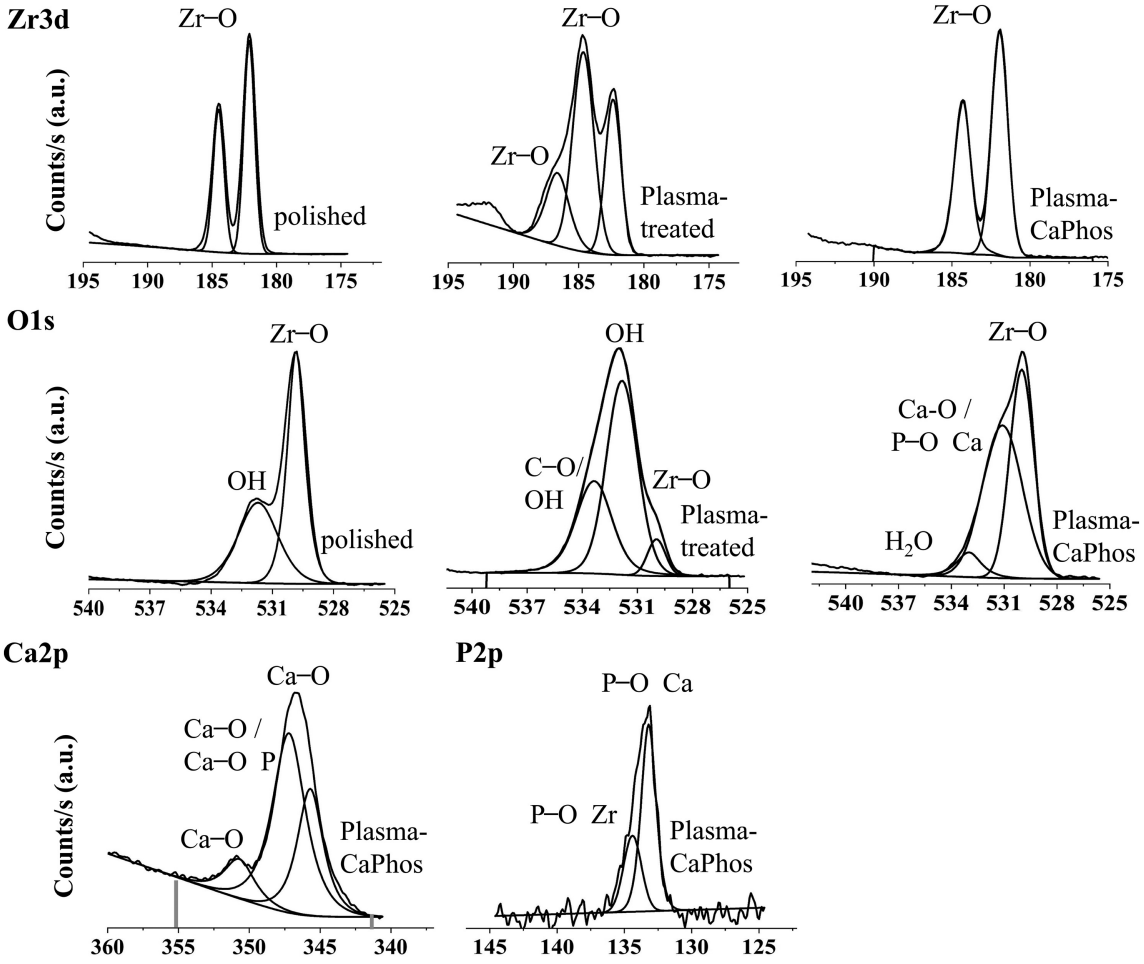

Fig. 4. Zr3d and O1s XPS spectra for polished, plasma-treated and plasma-CaPhos samples. Ca2p and P2p for plasma-CaPhos sample.

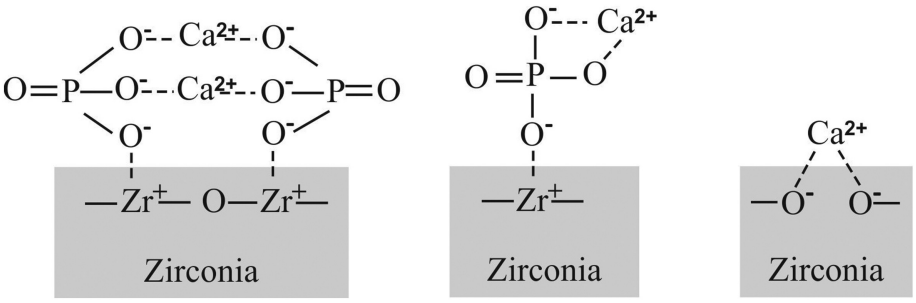

Fig. 5. Schematic representation of the interactions of calcium and phosphate on the surface of functionalized zirconia (plasma-CaPhos sample).

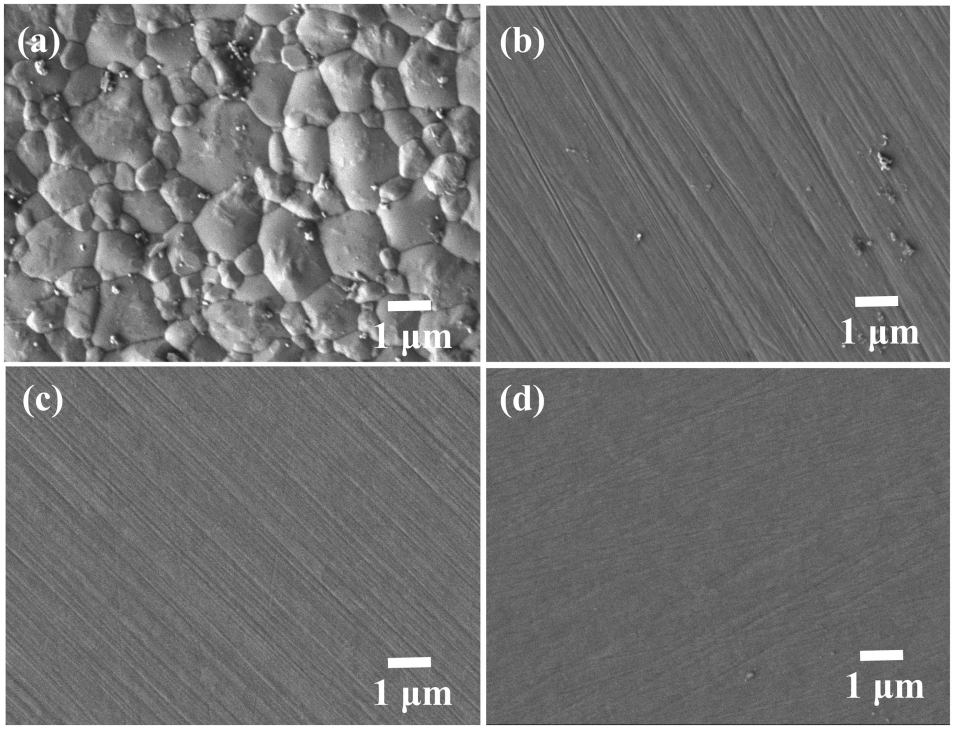

Fig. 6. Zirconia surfaces (a) untreated, (b) polished, (c) plasma-treated, (d) plasma-CaPhos.

negatively with protein at the nanoscale. Nanotopography of materials relating with biological systems like proteins and cells is critical to reach a successful interaction such as bonding, in the case of proteins, or adhesion for cells [33]. Therefore, it is critical to know how different process and surface treatments can affect topography. For this, we studied the topography of our samples through the process, SEM and AFM were the techniques used to do it. SEM images were taken at low magnification to observe the surfaces transition from the unpolished sample to the plasma-CaPhos sample (Fig. 6), the one to be coated with the protein. Unpolished surface shows the microstructure, which is erased by the polishing processes and substituted by scratches. Plasma-treated sample exhibit a smoother surface as well as the plasma-CaPhos.

AFM was used to investigate the surfaces at the nanoscale. In contrast to SEM, AFM allows us to get more analytical information about topography. For this, the polished, plasma-treated and plasma-CaPhos samples were analyzed using two specimens per sample and three images per specimen. Table II shows a summary of the analytical results. AFM images can be found in the complementary information, Fig. S2.

The three samples have very close values; a nanometric RMS roughness below 2 nm, a maximum height approximately to 10 nm and the average height close to 5 nm. The plasma-treated sample shows a slight decrease in these values, it is very low but still could be considered as a plasma mild etching effect. Contrary, plasma-CaPhos exhibit a little increasing, surely due to functionalization. In brief, all samples exhibit a nanotopography suitable to interact with proteins and cells, as mentioned by Lord [33].

Table II
AFM nanotopography analysis.

	Polished	Plasma-treated	Plasma-CaPhos
RMS roughness (nm)	1.76 ± 0.4	1.29 ± 0.3	1.66 ± 0.2
Maximum Z (height) value (nm)	10.87 ± 0.9	9.87 ± 0.8	10.93 ± 0.1
Average height (nm)	5.64 ± 0.1	5.76 ± 0.1	4.99 ± 0.5

3.3. Biofunctionalization with Ln-5 protein

3.3.1. Protein coating

Biofunctionalization of zirconia was accomplished by the Ln-5 protein adsorption on the treated surface. In order to test the effectiveness of surface treatments three samples were used, the polished, plasma-treated and plasma-CaPhos. We used two different protein concentrations, 0.08 µM and 0.016 µM, to better understand its behavior. Results were investigated by SEM, AFM and XPS.

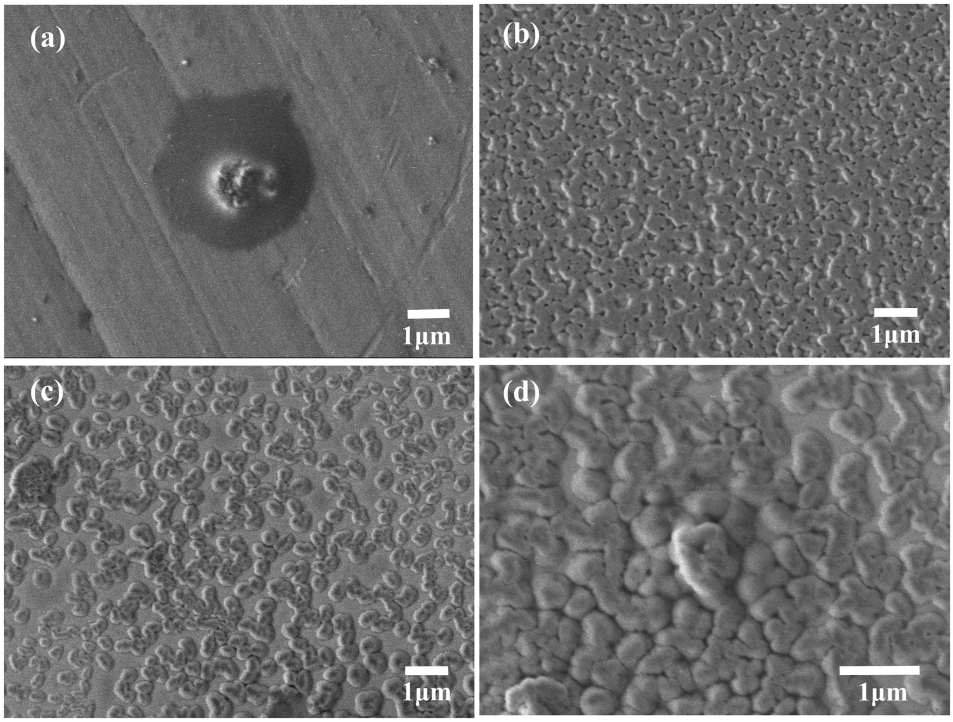

Fig. 7. SEM images of bionfunctionalized sample with Ln-5 protein. (a) Plasma-treated (0.08 μM Ln-5), (b) Plasma-CaPhos (0.08 μM Ln-5), (c) and (d) Plasma-CaPhos (0.016 μM Ln-5) at different magnifications. All bars 1 μm.

Ln-5 do not attached to the polished sample (image not shown), the plasma-treated surface was not covered neither, however, some protein aggregates were observed over its surface (Fig. 7a). In contrast, in the Plasma-CaPhos surface with 0.08 μM Ln-5, the protein was homogeneously attached over the whole surface forming a kind of protein network (Fig. 7b). The Plasma-CaPhos surface with 0.016 μM Ln-5 also exhibits protein homogeneously distributed over the surface, but due to the lower concentration, the protein aggregates are more spaced (Fig. 7c). Details of the protein morphology are shown in Fig. 7d (lower amount at higher magnification, 20,000×), whereby a well-defined three-dimensional globular and a little squashed shape with smooth contours, typical of proteins could be observed. The superficial globular sizes are around 200 to 400 nm, suggesting the formation of oligomers, since the size of an extended molecule of Ln-5 is at most 120 nm [44].

With SEM we only could observe the protein oligomers formed over the surface, however, it was impossible for us to see more details of the oligomer structure (Fig. 8a). AFM analysis allows us to scrutinize at the nanoscale these protein structures. The Fig. 8b shows an AFM image taken to a protein aggregate (as those shown in 8a) over a surface of 500 × 500 nm^2. In contrast to SEM, this image (8b) shows what appear to be details of single proteins, since globular shapes minor than 50 nm are present. Therefore AFM supports that the aggregates observed in SEM are indeed formed by smaller protein nanostructures.

To better understand the protein adsorption by the functionalized zirconia surface it is important to study the Ln-5 structure. In brief, Ln-5 is a protein composed of three chains α3, β3 and γ2, containing different domains, L4, LN, LE and LG [45,46], as illustrated in Fig. S1. Laminin has both hydrophobic and hydrophilic sites and the highest anionic charge has been localized in the LG modules. The overall isoelectric point is 5.57 (BioLamina), meaning that at a physiological pH, the protein has a negative charge. However, different isoelectric points for the different domains have been reported. For instance, positive domains can be found at physiological pH such as L4 and LE [47]. As protein adsorption was carried out at a physiological pH of 7.4, the positively charged domains on Ln-5 would favor charge interactions with the negatively charged surface of the plasma-CaPhos samples

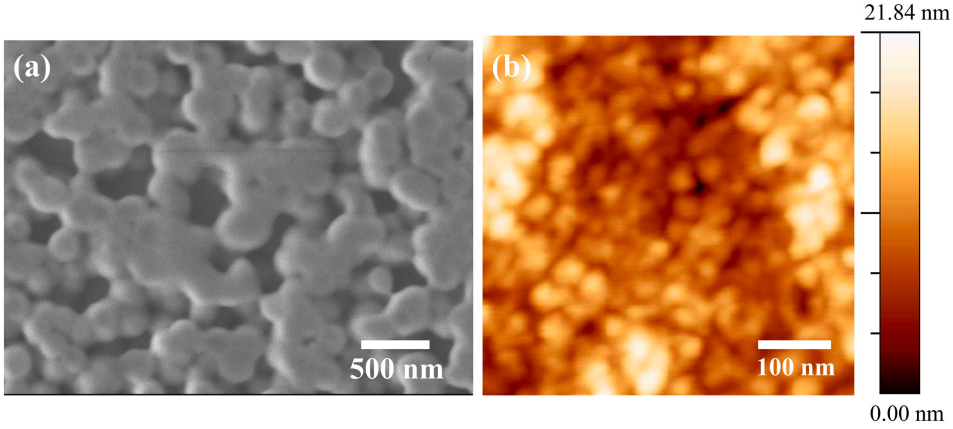

Fig. 8. Plasma-CaPhos-Ln sample (0.08 μM Ln-5) observed by (a) SEM and (b) AFM.

Table III
Depth profile of elemental composition as a percentage of plasma treated zirconia, functionalized with calcium-phosphate and laminin-5 (Plasma-CaPhos-Ln, 0.08 μM).

	Atomic %						
	Depth (nm)	C1s	N1s	Ca2p	P2p	Zr3d	O1s	Y3d
Plasma-CaPhos-Ln	0	37.23	1.55	2.04	9.12	3.24	46.54	0.25
	10	3.87	1.23	12.20	0.47	2.18	79.78	0.26
	19	2.53	0.85	14.35	0.99	7.60	73.09	0.58
	26	1.96	0.45	8.58	0.83	27.09	58.93	2.13
	34	2.87	0.36	8.22	0.38	27.52	58.35	2.27

(−19.5 mV).

The adsorption of the protein at the plasma-CaPhos sample was assisted not only by the addition of calcium and phosphate ions, but also by the previous short plasma treatment before protein adsorption, which probably breaks atomic bonds creating active sites and leaving a charged and prone to reaction surface, in short, activating the surface. This is supported experimentally since some experimental trials without the short (2-minute) plasma treatment failed to attach the protein appropriately.

3.3.2. Chemical composition of biofunctionalized zirconia

We measured the elemental composition and binding energies by XPS, with a depth profile extending to 38 nm, to provide chemical evidence of biofunctionalization at the surface of zirconia substrate with Ln-5. A single measurement of the atomic percentage of elements present on the plasma-CaPhos-Ln sample at different depths is presented in Table III. The detected C and N elements are likely to be part of the attached protein. However, when the percentage of C on the surface of the Plasma-CaPhos sample, which was related to environmental contamination (Table I), is contrasted with C measured in biofunctionalized Plasma-CaPhos-Ln (Table III), the latter constitutes a much greater amount, suggesting that it derives from adsorbed protein. The detection of N reinforces the existence of protein material on the surface. The considerable amount of P at the first 10 nm is probably partly derived from phosphate buffer, used to load the protein, while the other part comes from the functionalization layer. At depths above 10 nm, the percentage of Ca increased notably, denoting the functionalization layer and according to XPS, it may be bound to surface oxygens of zirconia and to deposited phosphates. The Zr and Y elements increased considerably at depths below 26 nm, which is consistent with the zirconia substrate. Oxygen percentage was the highest and predominates between 9 and 20 nm; the high contribution of O was expected, as this is a component of protein, phosphates and zirconia substrate.

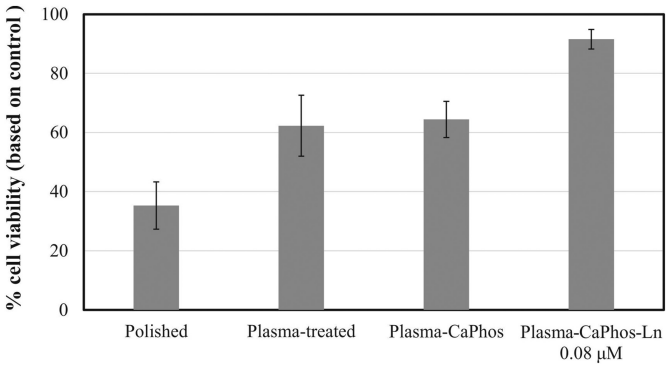

Fig. 10. Cell viability for different zirconia surfaces.

Considering the percentage of the elements along the depth profile, the presence of two functionalization layers across the zirconia substrate is probable. The upper layer, consisting of the protein Ln-5 comprises about the first 9 nm and the layer with calcium-phosphate appears to be present from 9 to 26 nm. Below a depth of 26 nm, Zr and Y notably increase, whereas P and Ca decrease.

As C and N are part of the protein, the binding energies of these elements were analyzed in Plasma-CaPhos-Ln sample, Fig. 9. The binding energies measured for the C1s (Fig. 9a) are shown at the four peaks; at 284.7 eV (C1), corresponding to C—H and C—C bonds [20,25]; the peak at 286.02 eV (C2), corresponding to C—O, C—N, C—S [20]; the peak at 292.6 eV (C3), related to the O=C—O bond and the peak at 295.4 eV (C4), related to the C—O bond. Additionally, the characteristic binding energy for N1s was detected at 399.6 eV (Fig. 9b), which is assigned to the amine group in proteins. The binding energies of C1s and N1s provide evidence of functional groups belonging to the protein Ln-5 attached to the zirconia surface and corroborates successful biofunctionalization. A similar N1s binding energy signal (399.9 ± 0.1 eV) was reported in a study by Vallee et al. [20].

3.4. Cell viability and adhesion

3.4.1. Cell viability

Cell viability was tested in polished, plasma-treated, plasma-CaPhos

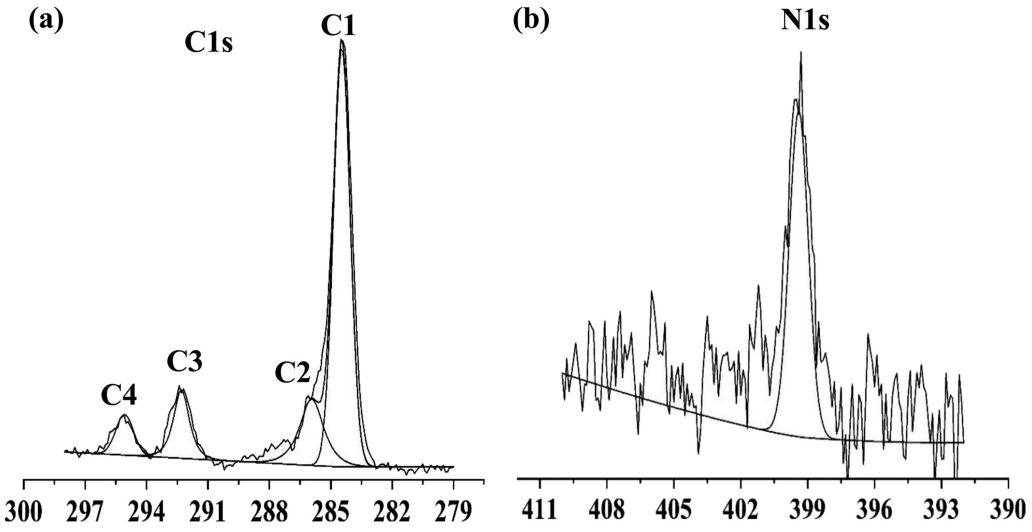

Fig. 9. XPS spectra of (a) C and (b) N detected in Plasma-CaPhos-Ln sample.

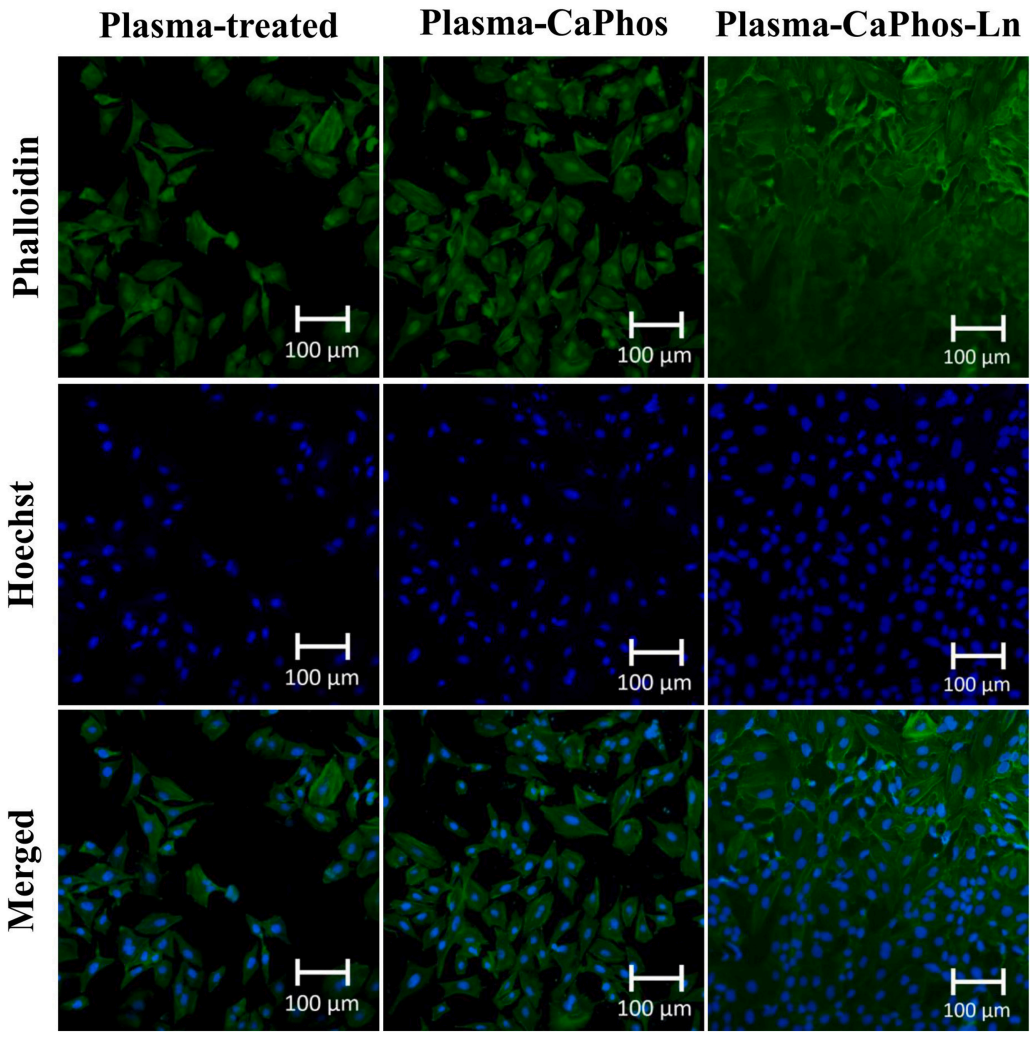

Fig. 11. Cell adhesion to modified zirconia surfaces after 24 h. F-actin staining (Phalloidin) and Nucleus staining (Hoechst). 20×. (For interpretation of the references to color in this figure, the reader is referred to the web version of this article.)

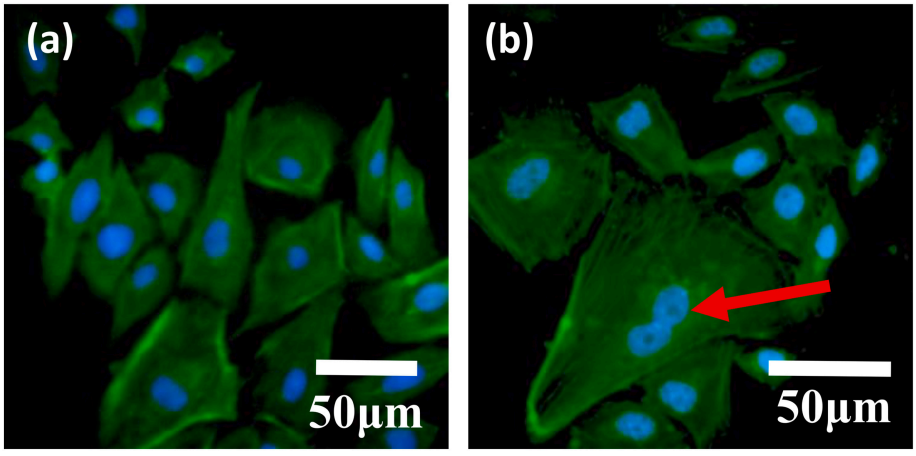

Fig. 12. Cells adhered to a Plasma-CaPhos-Ln sample, F-actin staining (phalloidin) and Nucleus staining (Hoechst) at (a) 50× and (b) 63×. (For interpretation of the references to color in this figure, the reader is referred to the web version of this article.)

and plasma-CaPhos-Ln samples (0.08 µM), Fig. 10. The viability of the latter sample reached values closer to the control (92% ± 3), indicating that protein coating favors the attachment of epithelial cells, as much lower values were observed for the plasma-treated and plasma-CaPhos samples (62% ± 10 and 64% ± 6, respectively). The polished sample manifested the lowest viability of 35% (± 8). Based on these results, to some extent, all surface samples were able to sustain cell viability with enhanced response at the sample coated with the Ln-5 protein. These results concur with a comparable study, where the deposition of laminin on a hydroxyapatite surface enhanced the attachment and

spreading of MC3T3-E1 osteoblastic cells [48].

3.4.2. Cell adhesion

Cell morphology and adhesion to the plasma-treated, plasma-CaPhos and plasma-CaPhos-Ln (0.08 μM) surfaces was corroborated by confocal optic microscopy on stained cells with Hoechst (blue, nucleus) and with phalloidin (green, F-actin of cytoskeleton). The polished sample was not analyzed because the MTT assay revealed low cell viability. The fluorescent images of the adhered CaCo2 epithelial cells after 24 h culture are presented in Fig. 11, which covered a field area of 640 × 640 μm^2. The images reveal that the plasma-CaPhos-Ln sample has more attached cells, compared to plasma-treated and plasma-CaPhos samples. On the previous surface, we counted an average cell density of 189 ± 25 cells/area by means of Image J (software), whereas in the plasma-CaPhos and plasma-treated samples, a density of 96 ± 21 and 78 ± 15 cells/area was obtained. This clearly showed that deposition of Ln protein on the surface of Plasma-CaPhos favors the attachment of cells, which were viable as demonstrated by MTT assay. Also, the spread morphology of cells (shown by green cytoskeleton) is an indication that cells adhere and proliferate over the three surfaces with greatest viability in the single coating of protein [37].

The attachment of cells to the Ln-5 protein can be explained trough the protein domain LG3 which promotes adhesion and spreading of epithelial cells on the surface via the integrins α3β1 [32,49].

To provide a close up of cell morphology on the plasma-CaPhos-Ln surface, cells were observed at greater magnification: Fig. 12. The images show the spread morphology of adhered cells to the surface, and also, in Fig. 12b, there is a clear process of cellular mitosis (red arrow) that suggests the proliferation of cells over the biofunctionalized zirconia surface.

4. Conclusion

Argon plasma treatment changed the physicochemical properties of the zirconia surface by mild etching and by the incorporation of O through functional groups that considerably enhanced its surface energy and wettability. This chemical modification enabled subsequent surface functionalization with calcium and phosphate ions. Biofunctionalization with Ln-5 protein by means of electrostatic interactions was also favored by a short second plasma treatment which activated the surface probably by breaking some atomic bonds. A homogenous film of Ln-5 protein over the functionalized zirconia surface with three-dimensional globular shape was confirmed by SEM and AFM. The presence of Ca, P, O elements on functionalized surfaces was evidenced by Confocal Raman microsocopy and XPS, along with the characteristic binding energies for Ca—O—P, P—O—Zr and Ca—O bonds revealed by XPS. This confirmed the proposed interaction of the functionalization of zirconia surface with calcium phosphate. Similarly, a major percentage of C on biofunctionalized samples and the presence of N with typical binding energy for amine group, corroborated the attachment of Ln-5 protein to the surface. The functionalization treatments improved zirconia surface bioactivity, with notable improvement in viability and adhesion of epithelial cells (CaCo2), on surfaces where Ln protein was deposited, resulting in visible cell proliferation. Thus, this study provides a suitable process for the biofunctionalization of inert bioceramics such as zirconia, with promising implant applications.

CRediT authorship contribution statement

Lillian V. Tapia-Lopez: Methodology, Validation, Formal analysis, Investigation, Data curation, Writing - original draft, Visualization. **Hilda E. Esparza-Ponce:** Writing - review & editing, Supervision, Visualization. **Antonia Luna-Velasco:** Resources, Writing - review & editing, Supervision, Visualization. **Perla E. Garcia-Casillas:** Validation. **Homero Castro-Carmona:** Conceptualization. **Javier S. Castro:** Conceptualization, Resources, Writing - review & editing, Supervision, Project administration, Funding acquisition.

Declaration of competing interest

The authors declare that they have no known competing financial interests or personal relationships that could have appeared to influence the work reported in this paper.

Acknowledgments

This work was supported by CONACYT (grant SEP CB 2014-241001). L. Tapia acknowledges CONACYT for the academic grant 449042. Authors thank M. Mendoza-Duarte, K. Campos-Venegas, L.G. Silva-Vidaurri, L. Bautista, M. Mendoza, W. Antunez, I. Murillo and R. Farias for their contributions to the characterization analysis.

Appendix A. Supplementary data

Supplementary data to this article can be found online at https://doi.org/10.1016/j.surfcoat.2020.126307.

References

[1] Y. Zhou, C. Wu, J. Chang, Bioceramics to regulate stem cells and their microenvironment for tissue regeneration, Mater. Today 24 (2019) 41–56, https://doi.org/10.1016/j.mattod.2018.07.016.
[2] M. Liu, J. Zhou, Y. Yang, M. Zheng, J. Yang, J. Tan, Surface modification of zirconia with polydopamine to enhance fibroblast response and decrease bacterial activity in vitro: a potential technique for soft tissue engineering applications, Colloids Surf. B: Biointerfaces 136 (2015) 74–83, https://doi.org/10.1016/j.colsurfb.2015.06.047.
[3] O. Carvalho, F. Sousa, S. Madeira, F.S. Silva, G. Miranda, HAp-functionalized zirconia surfaces via hybrid laser process for dental applications, Opt. Laser Technol. 106 (2018) 157–167, https://doi.org/10.1016/j.optlastec.2018.03.017.
[4] M. Dehestani, D. Zemlyanov, E. Adolfsson, L.A. Stanciu, Improving bioactivity of inert bioceramics by a novel Mg-incorporated solution treatment, Appl. Surf. Sci. 425 (2017) 564–575, https://doi.org/10.1016/j.apsusc.2017.07.009.
[5] T.J. Thorson, R.E. Gurlin, E.L. Botvinick, A. Mohraz, Bijel-templated implantable biomaterials for enhancing tissue integration and vascularization, Acta Biomater. 94 (2019) 173–182, https://doi.org/10.1016/j.actbio.2019.06.031.
[6] J.M. Anderson, A. Rodriguez, D.T. Chang, Foreign body reaction to biomaterials, Semin. Immunol. 20 (2008) 86–100, https://doi.org/10.1016/j.smim.2007.11.004.
[7] E. Mariani, G. Lisignoli, R. Maria, L. Pulsatelli, Biomaterials: foreign bodies or tuners for the immune response? Int. J. Mol. Sci. 20 (2019), https://doi.org/10.3390/ijms20030636.
[8] W. Winter, D. Klein, M. Karl, Micromotion of dental implants: basic mechanical considerations, J. Med. Eng. 2013 (2013), https://doi.org/10.1155/2013/265412.
[9] J. Adhikari, P. Saha, A. Sinha, 14. Surface modification of metallic bone implants—polymer and polymer-assisted coating for bone in-growth, Fundam. Biomater. Met, Elsevier Ltd, 2017, pp. 299–320, , https://doi.org/10.1016/B978-0-08-102205-4.00014-3.
[10] X. Zhao, Introduction to bioactive materials in medicine, Bioact. Mater. Med. (2011) 1–13, https://doi.org/10.1533/9780857092939.1.
[11] S. Nour, N. Baheiraei, R. Imani, N. Rabiee, M. Khodaei, Bioactive materials: a comprehensive review on interactions with biological microenvironment based on the immune response, J. Bionic Eng. 16 (2019) 563–581, https://doi.org/10.1007/s42235-019-0046-z.
[12] N.A. Peppas, J.R. Clegg, The challenge to improve the response of biomaterials to the physiological environment, Regen. Biomater. (2016) 67–71, https://doi.org/10.1093/rb/rbw012.
[13] M. Vallet-Regí, Evolution of bioceramics within the field of biomaterials, Comptes Rendus Chim 13 (2010) 174–185, https://doi.org/10.1016/j.crci.2009.03.004.
[14] K.I. Sunarso, Riki Toita, Kanji Tsuru, Immobilization of Calcium and Phosphate Ions Improves the Osteoconductivity of Titanium Implants, (2016), pp. 291–298, https://doi.org/10.1016/j.msec.2016.05.090.
[15] D. Almasi, N. Iqbal, M. Sadeghi, I. Sudin, M. Rafiq, A. Kadir, T. Kamarul, Preparation methods for improving PEEK's bioactivity for orthopedic and dental application: a review, Int. J. Biomater. 2016 (2016) 1–12 (10.115/2016/82022653).
[16] M.I. Froimson, J. Garino, A. Machenaud, J.P. Vidalain, Minimum 10-year results of a tapered, titanium, hydroxyapatite-coated hip stem an independent review, J. Arthroplast. 22 (2007) 1–7, https://doi.org/10.1016/j.arth.2006.03.003.
[17] G. Soon, B. Pingguan-Murphy, K.W. Lai, S.A. Akbar, Review of zirconia-based bioceramic: surface modification and cellular response, Ceram. Int. 42 (2016) 12543–12555, https://doi.org/10.1016/j.ceramint.2016.05.077.
[18] T. Murakhami, S. Takemoto, N. Nishayama, M. Aida, Zirconia surface modification by a novel zirconia bonding system and its adhesion mechanism, Dent. Mater. 33 (2017) 1371–1380, https://doi.org/10.1016/j.dental.2017.09.001.
[19] E. Fernandez-Garcia, X. Chen, C.F. Gutierrez-Gonzalez, A. Fernandez, S. Lopez-

Esteban, C. Aparicio, Peptide-functionalized zirconia and new zirconia/titanium biocermets for dental applications, J. Dent. 43 (2015) 1162–1174, https://doi.org/10.1016/j.jdent.2015.06.002.
[20] A. Vallée, M.G. Faga, F. Mussano, F. Catalano, E. Tolosano, S. Carossa, F. Altruda, G. Martra, Colloids and surfaces B: biointerfaces alumina – zirconia composites functionalized with laminin-1 and laminin-5 for dentistry: effect of protein adsorption on cellular response, Colloids Surf. B: Biointerfaces 114 (2014) 284–293, https://doi.org/10.1016/j.colsurfb.2013.09.053.
[21] M. Tallarico, L. Canullo, M. Caneva, M. Özcan, Microbial colonization at the implant-abutment interface and its possible influence on periimplantitis: a systematic review, J. Prosthodont. Res. (2017), https://doi.org/10.1016/j.jpor.2017.03.001.
[22] H. Algraffee, F. Borumandi, L. Cascarini, Peri-implantitis, Br. J. Oral Maxillofac. Surg. 50 (2012) 689–694, https://doi.org/10.1016/j.bjoms.2011.11.020.
[23] C. Caravaca, L. Shi, S. Balvay, P. Rivory, E. Laurenceau, Y. Chevolot, D. Hartmann, L. Gremillard, J. Chevalier, Direct silanization of zirconia for increased biointegration, Acta Biomater. (2016), https://doi.org/10.1016/j.actbio.2016.09.034.
[24] S. Cheruthazhekatt, P. Slaví, J. Havel, Gas plasmas and plasma modified materials in medicine, J. Appl. Biomed. 8 (2010) 55–66, https://doi.org/10.2478/v10136-009-0013-9.
[25] T. Jacobs, N. De Geyter, R. Morent, T. Desmet, P. Dubruel, C. Leys, Plasma treatment of polycaprolactone at medium pressure, Surf. Coat. Technol. 205 (2011) 543–547, https://doi.org/10.1016/j.surfcoat.2011.02.012.
[26] R. Bitar, M. Asadian, S. Van Vrekhem, P. Cools, H. Declercq, R. Morent, N. De Geyter, Local plasma activation of PS films with a defined design for biomedical use, Surf. Coat. Technol. 350 (2018) 985–996, https://doi.org/10.1016/j.surfcoat.2018.03.041.
[27] D. Kontziampasis, T. Trantidou, A. Regoutz, E.J. Humphrey, D. Carta, C.M. Terracciano, T. Prodromakis, Effects of Ar and O2 plasma etching on parylene C: topography versus surface chemistry and the impact on cell viability, Plasma Process. Polym. 13 (2016) 324–333, https://doi.org/10.1002/ppap.201500053.
[28] R.R.W.-H.L. Ching-Yee Loo, A review of chemical surface modification of bioceramics: effects on protein adsorption and cellular response, Colloids Surf. B: Biointerfaces 122 (2014) 823–834, https://doi.org/10.1016/j.colsurfb.2014.07.029.
[29] W. He, Z. Ma, T. Yong, W. Eong, S. Ramakrishna, Fabrication of collagen-coated biodegradable polymer nanofiber mesh and its potential for endothelial cells growth, Biomaterials 26 (2005) 7606–7615, https://doi.org/10.1016/j.biomaterials.2005.05.049.
[30] C.G. Cornelissen, M. Dietrich, K. Gromann, J. Frese, S. Krueger, J.S. Sachweh, S. Jockenhoevel, Fibronectin coating of oxygenator membranes enhances endothelial cell attachment, Biomed. Eng. Online 12 (2013) 1–8, https://doi.org/10.1186/1475-925X-12-7.
[31] E. Hintermann, V. Quaranta, Epithelial cell motility on laminin-5: regulation by matrix assembly, proteolysis, integrins and erbB receptors, Matrix Biol. 23 (2004) 75–85, https://doi.org/10.1016/j.matbio.2004.03.001.
[32] I. Atsuta, T. Yamaza, M. Yoshinrari, T. Goto, Kido, T. Kagiya, S. Mino, M. Shimono, T. Tanaka, Ultrastructural localization of laminin-5 (chain) in the rat peri-implant oral mucosa around a titanium-dental implant by immuno-electron microscopy, Biomaterials. 26 (2005) 6280–6287. doi:https://doi.org/10.1016/j.biomaterials.2005.03.046.
[33] M.S. Lord, M. Foss, F. Besenbacher, Influence of nanoscale surface topography on protein adsorption and cellular response, Nano Today 5 (2010) 66–78, https://doi.org/10.1016/j.nantod.2010.01.001.
[34] H.M.-R. Kasra Tabari, Sepanta Hosseinpour, The impact of plasma treatment of Cercon ® zirconia ceramics on adhesion to resin composite, Laser Appl. Med. Sci. Res. Cent. 8 (2017) S56–S61, https://doi.org/10.15171/jlms.2017.s11.
[35] Y. Liu, J. Hsieh, Y. Chen, L. Kang, Promoting porcelain – zirconia bonding using different atmospheric pressure gas plasmas, Dent. Mater. (2018) 1–11, https://doi.org/10.1016/j.dental.2018.05.004.
[36] G.B. Valverde, P.G. Coelho, M.N. Janal, R.M. Carvalho, V.P. Thompson, K. Weltemann, N.R.F.A. Silva, Surface characterisation and bonding of Y-TZP following non-thermal plasma treatment, J. Dent. 41 (2012) 51–59, https://doi.org/10.1016/j.jdent.2012.10.002.
[37] L. Fernandes, R. Aquino, D. Carvalho, A. Capaldo, E. Pecoraro, R. Salomão, E. Trovatti, Mullite cytotoxicity and cell adhesion studies, J. Mater. Res. Technol. 8 (2019) 2565–2572 (doi:10.1016/).
[38] J. Nawrocki, A. Mccormick, P.W. Carr, Review chemistry of zirconia and its use in chromatography, J. Chromatogr. A 657 (1993) 229–282.
[39] D.I. Torres, J. Llopis, Infrared photoluminescence and Raman spectra in the Y2O3-ZrO2 system, Superlattice. Microst. 45 (2009) 482–488, https://doi.org/10.1016/j.spmi.2008.11.020.
[40] C.G.A.A. Lopera, A. Montoya, I.D. Velez SM Robledo, Synthesis of calcium phosphate nanostructures by combustion in solution as a potential encapsulant system of drugs with photodynamic properties for the treatment of cutaneous leishmaniasis, Photodiagn. Photodyn. Ther. 21 (2018) 138–146, https://doi.org/10.1016/j.pdpdt.2017.11.017.
[41] D. Yamini, G. Devanand Venkatasubbu, J. Kumar, V. Ramakrishnan, Raman scattering studies on PEG functionalized hydroxyapatite nanoparticles, Spectrochim. Acta - Part A Mol. Biomol. Spectrosc. 117 (2014) 299–303, https://doi.org/10.1016/j.saa.2013.07.064.
[42] P.N. De Aza, C. Santos, A. Pazo, L. Artu, Vibrational properties of calcium phosphate compounds. 1. Raman Spectrum of -tricalcium phosphate, Chem. Mater. 4756 (1997) 912–915.
[43] C.K.I.A. Karampas, Characterization of calcium phosphates mixtures, Vib. Spectrosc. 64 (2013) 126–133, https://doi.org/10.1016/j.vibspec.2012.11.003.
[44] K. Beck, I. Hunter, J. Engel, Structure and function: anatomy of a multidomain glycoprotein, FASEB J. 4 (2016) 148–160, https://doi.org/10.1096/fasebj.4.2.2404817.
[45] H. Schneider, C. Mühle, F. Pacho, Biological function of laminin-5 and pathogenic impact of its deficiency, Eur. J. Cell Biol. 86 (2007) 701–717, https://doi.org/10.1016/j.ejcb.2006.07.004.
[46] M. Aumailley, L. Bruckner-Tuderman, W.G. Carter, R. Deutzmann, D. Edgar, P. Ekblom, J. Engel, E. Engvall, E. Hohenester, J.C.R. Jones, H.K. Kleinman, M.P. Marinkovich, G.R. Martin, U. Mayer, G. Meneguzzi, J.H. Miner, K. Miyazaki, M. Patarroyo, M. Paulsson, V. Quaranta, J.R. Sanes, T. Sasaki, K. Sekiguchi, L.M. Sorokin, J.F. Talts, K. Tryggvason, J. Uitto, I. Virtanen, K. Von Der Mark, U.M. Wewer, Y. Yamada, P.D. Yurchenco, A simplified laminin nomenclature, Matrix Biol. 24 (2005) 326–332, https://doi.org/10.1016/j.matbio.2005.05.006.
[47] T. Ogawa, Y. Tsubota, J. Hashimoto, Y. Kariya, K. Miyazaki, The short arm of laminin γ2 chain of laminin-5 (laminin-332) binds syndecan-1 and regulates cellular adhesion and migration by suppressing phosphorylation of integrin β 4 chain, Mol. Biol. Cell 18 (2007) 1621–1633, https://doi.org/10.1091/mbc.E06.
[48] H. Fujita, T.A. Kudo, H. Kanetaka, T. Miyazaki, M. Hashimoto, M. Kawashita, Adsorption of laminin on hydroxyapatite and alumina and the MC3T3-E1 cell response, ACS Biomater. Sci. Eng. 2 (2016) 1162–1168, https://doi.org/10.1021/acsbiomaterials.6b00190.
[49] J.M. Kim, W.H. Park, B.M. Min, The PPFLMLLKGSTR motif in globular domain 3 of the human laminin-5 α3 chain is crucial for integrin α3β1 binding and cell adhesion, Exp. Cell Res. 304 (2005) 317–327, https://doi.org/10.1016/j.yexcr.2004.11.009.